360° domain walls in magnetic thin films with uniaxial and random anisotropy

N. Chowdhury,[1,*] W. Kleemann,[2] O. Petracic,[3] F. Kronast,[4] A. Doran,[5] A. Scholl,[5] S. Cardoso,[6] P. Freitas,[6] and S. Bedanta[1,†]

[1]*Laboratory for Nanomagnetism and Magnetic Materials, School of Physics, National Institute of Science Education and Research, HBNI, Jatni 752050, India*

[2]*Angewandte Physik, Universität Duisburg-Essen, 47048 Duisburg, Germany*

[3]*Jülich Centre for Neutron Science and Peter Grünberg Institut, JARA-FIT Forschungszentrum Jülich GmbH, 52425 Jülich, Germany*

[4]*Helmholtz-Zentrum Berlin für Materialien und Energie, Albert-Einstein-Strasse 15, 12489 Berlin, Germany*

[5]*Advanced Light Source, Lawrence Berkeley National Laboratory, 1 Cyclotron Road, Berkeley, California 94720, USA*

[6]*INESC-Microsystems and Nanotechnologies and Instituto Superior Tecnico, Universidade de Lisboa, Lisbon 1000, Portugal*

(Received 27 July 2017; revised manuscript received 12 September 2018; published 24 October 2018)

X-ray photoemission electron microscopy (XPEEM) and magneto-optic Kerr effect (MOKE) microscopy have been performed on a metal-insulator multilayer of $[Co_{80}Fe_{20}(t = 1.8\ nm)/Al_2O_3(3\ nm)]_9$ to image 360° domain walls (DWs) along easy and hard axes, respectively. Their creation and annihilation can be directly visualized under application of a magnetic field. XPEEM experiments and micromagnetic simulations show that 360° DWs occur through the merger of 180° DWs of opposite chiralities along the easy axis. They are stable even under application of large magnetic fields. Formation of 360° DWs observed along the hard axis is attributed to symmetry breaking of the coherent spin rotation. Their formation in metal-insulator multilayers is explained as being due to the presence of an orientational dispersion of anisotropy axes in the film grains that is comparable to an overall uniaxial anisotropy term. Our results are confirmed numerically using micromagnetic simulations.

DOI: 10.1103/PhysRevB.98.134440

I. INTRODUCTION

Magnetic multilayers comprising ferromagnetic and nonmagnetic layers have been intensely studied to understand various fundamental physics problems and because of their potential use in magnetoresistive device applications [1,2]. It is desirable for such devices to exhibit a reliable and uniform magnetization reversal. Hence, to improve and engineer the performance of these devices, it is necessary to understand the magnetic properties like the reversal process. Here, the role of domains is of paramount importance [3]. Their formation is well understood in terms of the minimization of the free energy. The total energy density E_{total} of a ferromagnetic material is the sum of exchange (E_{exch}), anisotropy (E_{anis}), Zeeman (E_{Zeem}), and demagnetization (E_{demag}) energy densities. E_{total} can be expressed as

$$\begin{aligned} E_{\text{total}} &= E_{\text{exch}} + E_{\text{anis}} + E_{\text{Zeem}} + E_{\text{demag}} \\ &= A(\nabla\phi)^2 + K_u \sin^2\phi - \mu_0 \mathbf{H}\cdot\mathbf{M} - \frac{1}{2}\mu_0 \mathbf{H}_{\text{demag}}\cdot\mathbf{M}, \end{aligned} \tag{1}$$

where A is the exchange constant, K_u is the uniaxial anisotropy constant, ϕ is the angle between the easy axis (EA) arising due to K_u and the magnetization M, H is the applied external magnetic field, and H_{demag} is the demagnetization field. K_u can be due to various origins such as magnetocrystalline, shape, surface, and strain anisotropies [4].

The uniaxial anisotropy can also be induced by the growth conditions, e.g., deposition under an oblique angle of incidence [5], preparation under an external magnetic field [6,7], and postannealing in the presence of a magnetic field [8]. It should be noted that magnetic films usually consist of grains with an average size, a certain size distribution, textures, and further morphological characteristics. This may lead to an orientational dispersion in the local anisotropies of the grains. The spatial fluctuations given by such orientational dispersion in local anisotropies may not be very strong; however, they may have a sizable global effect [9–11]. Precise measurements of such a spatial distribution of local anisotropy axes are difficult to obtain experimentally. Hence, the presence of such a distribution of local anisotropy axes is only indirectly observable. Alben *et al.* [11] proposed the so-called random-anisotropy (RA) model for amorphous ferromagnetic systems. The average anisotropy constant $\langle K_{ri}\rangle$ in a magnetic thin film with a polydispersive grain size distribution can be expressed with the help of the RA model as

$$\langle K_{ri}\rangle = \sum_i |K_{ri}| \left(\frac{D_i}{L_0}\right)^6, \tag{2}$$

where K_{ri} represents the local magnetic anisotropy of the grains, D_i is the diameter of the grains, and L_0 is the ferromagnetic exchange length [11,12]. The theory relies on the assumption that L_0 is larger than the average D_i. The RA model assumes that the magnitude of the local anisotropy of grains remains constant for each site i but varies spatially in its direction; that is, in reality the local anisotropy may have a directional dispersion. Thus, the total energy density E_{total} given in Eq. (1) for $\langle N\rangle$ randomly oriented exchange-coupled

*Present address: Department of Physics, Indian Institute of Technology Delhi, New Delhi 110016, India.

†sbedanta@niser.ac.in

grains will be modified to

$$E_{\text{total}} = A\sum_{i=1}^{N}(\nabla\phi_i)^2 + K_u sin^2\phi + \sum_{i=1}^{N} K_{ri}\sin^2(\phi-\phi_i) - \mu_0\mathbf{H}\cdot\sum_{i=1}^{N}\mathbf{M_i} - \frac{1}{2}\mu_0\mathbf{H}_{\text{demag}}\cdot\sum_{i=1}^{N}\mathbf{M_i}, \quad (3)$$

where ϕ_i denotes the direction of the local EA with respect to the global one and M_i is the magnetization vector of the ith grain.

Thus, the domain microstructure in a ferromagnetic thin film is governed by the energy given in Eq. (3). Such energy minimization leads to various shapes and sizes of domains. Further, this will have a decisive effect on the nature of the walls separating the domains. In ferromagnetic thin films or in general in magnetic nanostructures various types of domain walls (DWs) separate regions with different orientations of M, e.g., 90°, 180°, and 360° [13]. Among these the 360° DWs are particularly interesting because they separate regions (domains) with the same magnetization state [13].

The occurrence of 360° DWs is rare compared to, e.g., 180° DWs. Nevertheless, 360° DWs have been observed in exchange-coupled and exchange-biased systems when Bloch lines present in a 180° Néel wall get pinned at structural inhomogeneities or defects [2,14–17]. However, there have been reports in which 360° DWs are observed in the absence of any defects [18,19]. In such cases the formation of 360° DWs was possible due to the presence of the directional dispersion of EA in permalloy films. Such a dispersion in local anisotropy directions can be treated as a perturbation leading to opposite spin curling and hence formation of 360° DWs [18,20]. Hehn *et al.* predicted that the curling in a magnetic tunnel junction will depend on the variation of the local anisotropy, thermal fluctuations, and the torque created by the dipolar field of the hard magnetic layer [20]. In some cases, 360° DWs can be formed due to the magnetization rotation of nearby grains in opposite directions due to the presence of the distribution of the EA in the film [10,14,17].

Apart from thin films, several experimental and theoretical studies from various groups were performed to understand the origin of the observed 360° DWs in nanostructures like nanodots [20], rings [21], and nanowires [22,23]. These walls were also observed in composite nanostructures of Co and permalloy by magnetic force microscopy, scanning electron microscopy with polarization analysis [22], and Kerr microscopy [24]. It has been shown that once such 360° walls are formed, usually, it is very difficult to annihilate them even at relatively large magnetic fields [19]. Such a field stability would deteriorate the sensitivity of magnetoresistive sensors and hence must be avoided during reversal [17].

Even though 360° DWs have been considered to be undesirable in data storage technology, they are still being explored in view of possible applications. Diegel *et al.* proposed using the stability of 360° DWs as a future sensor application with certain spin valve geometries [24]. By applying magnetic fields perpendicular to the exchange bias direction concentric 360° DWs were formed in the free layer [17]. The authors of Ref. [17] claimed that their observation of nested 360° DWs can be used to count the number of magnetization reversals taking place in a device.

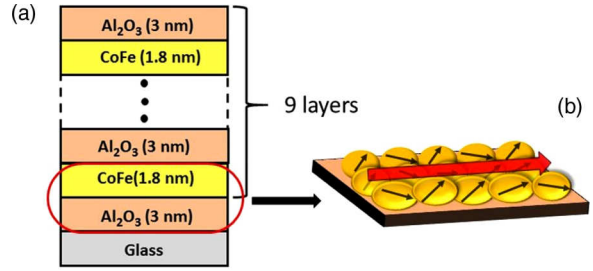

FIG. 1. (a) Schematic of the sample Al_2O_3(3 nm)/[$Co_{80}Fe_{20}$(t = 1.8 nm)/Al_2O_3(3 nm)]$_9$, (b) schematic showing the coalescence of nanoparticles to form continuous thin films with overall uniaxial (large red arrow) and random (small black arrows) anisotropy of the grains.

It is understood that 360° DWs are formed by the merger of two 180° Néel walls interacting magnetostatically. The present understanding of the origin and formation of 360° DWs is based on either the presence of defects or inhomogeneities in the grain magnetizations, which breaks the local symmetry of magnetization rotation. In this paper, we report the effect of random anisotropy (i.e., orientational dispersion in local easy axes) on the creation of 360° DWs. We discuss our results for a magnetic/nonmagnetic multilayer along the easy and hard axes using X-ray photoemission electron microscopy (XPEEM) and magneto-optic Kerr effect (MOKE) microscopy. Micromagnetic simulations using the object-oriented micromagnetic framework (OOMMF) software indicate that the competing effects of uniaxial and random anisotropy contributions lead to the occurrence of 360° DWs.

II. EXPERIMENTAL TECHNIQUES

Metal-insulator multilayers (MIMs) of [$Co_{80}Fe_{20}$(t = 1.8 nm)/Al_2O_3(3 nm)]$_9$ were prepared by Xe-ion beam sputtering on glass substrates [25]. The spacer layer Al_2O_3 was taken to suppress any direct exchange interaction between the consecutive CoFe layers. The schematic of the sample is shown in Fig. 1(a). In MIMs for low nominal CoFe thickness ($t \leqslant 1.6$ nm) discontinuous nanoparticulate layers emerge due to the pronounced Volmer-Weber growth mode [6,26]. However, the nominal CoFe layer thickness, $t = 1.8$ nm, warrants intraplanar percolation and hence exchange-dominated ferromagnetism in two dimensions. A small in-plane magnetic field of $\mu_0 H = 10$ mT was applied during the deposition of the layers. Such growth conditions were shown to induce an in-plane uniaxial anisotropy [6,7,27]. Since the magnetic field applied during deposition was relatively small, a certain random anisotropy due to the directional dispersion caused by the granularity of the film with an overall in-plane uniaxial anisotropy is expected. Figure 1(b) shows the pictorial representation of the uniaxial (large red arrow) and random (small black arrows) anisotropies present in the sample. This is also evident from the square and S-shaped hysteresis loops shown in Figs. 2(a) and 2(b) measured by longitudinal MOKE magnetometry along the EA and hard axis (HA), respectively. Note that the CoFe film deposited on a glass substrate is poly-

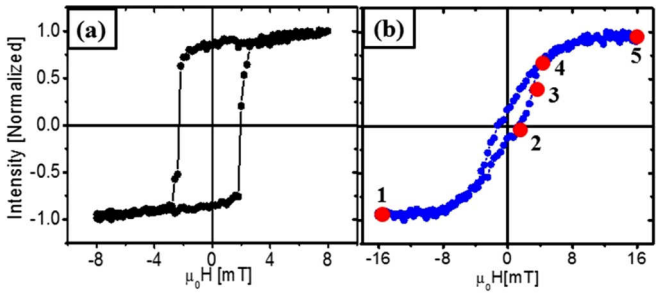

FIG. 2. LMOKE hysteresis loop for $[Co_{80}Fe_{20}(t = 1.8\ nm)/Al_2O_3(3\ nm)]_9$ measured by applying in-plane magnetic field along (a) EA and (b) HA measured at room temperature. The change in the loop from square to S shaped for EA to HA shows the presence of uniaxial anisotropy.

crystalline in nature and exhibits a clear in-plane anisotropy. During the growth of the films a magnetic field was applied, and this direction was found to be the EA.

Magnetic domain imaging along the EA was performed by XPEEM using x-ray magnetic circular dichroism at the L_3 absorption edge of Co (778 eV) [28]. These experiments were performed at beamline 11.0.1.1 at the Advanced Light Source in Berkeley, California, under magnetic field pulses and at the UE 49 SPEEM beamline at BESSY, Berlin, Germany, under variable magnetic fields with a specially designed setup [29]. In this paper we show the results obtained from BESSY. The magnetization reversal was studied using longitudinal MOKE (LMOKE) microscopy at a spatial resolution better than 1 μm manufactured by Evico Magnetics, Germany. It should be noted that in both XPEEM and Kerr microscopy the imaging is limited to the top layers because these are surface-sensitive techniques. Further, in order to understand the observed experimental results micromagnetic simulations were employed by using the OOMMF code [30].

III. RESULTS AND DISCUSSION

We have performed XPEEM under external magnetic fields on the MIM sample of $[Co_{80}Fe_{20}(t = 1.8\ nm)/Al_2O_3(3\ nm)]_9$. The external magnetic field was applied along the EA of the sample. First, the sample was saturated with a negative magnetic field. Then the field was switched towards the positive saturation direction, and imaging was performed at fields close to coercivity. Figures 3(a) and 3(b) show the domain images observed by

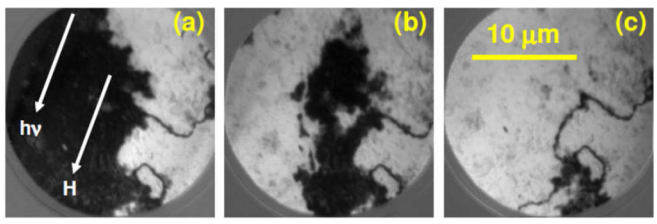

FIG. 3. XPEEM domain images of $[Co_{80}Fe_{20}(t = 1.8\ nm)/Al_2O_3(3\ nm)]_9$ at room temperature under subcoercive fields (a) $\mu_0 H = 1.9$ mT, (b) 1.95 mT, and (c) 1.95 mT. The image in (c) was taken a few seconds after the image in (b) was recorded.

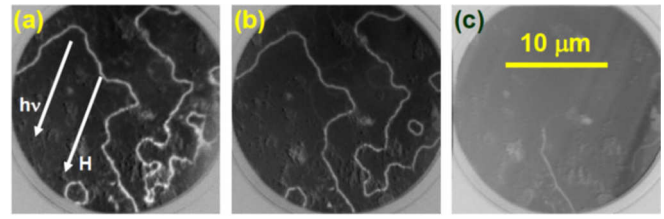

FIG. 4. XPEEM domain images of $[Co_{80}Fe_{20}(t = 1.8\ nm)/Al_2O_3(3\ nm)]_9$ at room temperature at magnetic fields of (a) $\mu_0 H = 5.48$ mT, (b) 9.12 mT, and (c) 23.7 mT.

XPEEM along EA at $\mu_0 H = 1.9$ and 1.95 mT, respectively. The image in Fig. 3(c) was recorded a few seconds after the image in Fig. 3(b). It is seen in Fig. 3(a) that two 180° domains are present, while in the center a threadlike 360° DW appears. With a further increase of the magnetic field we observed that the domains have shrunk further towards a positive magnetization state. By keeping the magnetic field constant the 180° domains merge and form a 360° DW, which is evidenced as the black thread in Fig. 3(c).

Figures 4(a)–4(c) show XPEEM domain images of $[Co_{80}Fe_{20}(t = 1.8\ nm)/Al_2O_3(3\ nm)]_9$ at room temperature at magnetic fields of $\mu_0 H = 5.48$, 9.12, and 23.7 mT, respectively. The 360° DWs are observed as white threads. It should be noted that the positive magnetization is defined as black. The typical field stability of the 360° DWs is clearly evidenced by the field-dependent images shown in Fig. 4. For better visualization see Video VS1 in the Supplemental Material [31], showing the annihilation of these walls under the increasing magnetic field imaged by XPEEM. It should be noticed that even at ~ 23.7 mT, 360° DWs exist, whereas the hysteresis loop (Fig. 2) for a measurement parallel to the EA indicates that saturation is reached. Although the 360° DWs shown in Fig. 4 hint that these DWs extend over several tens of micrometers, there exist smaller looplike 360° DWs as seen in Fig. 4(b). The pinning potential due to the defects present in the film may also have an effect on the 360° DWs. On the other hand, the dipolar repulsion between neighboring DWs may lead to such a nonlinear structure of 360° DWs [32].

Figures 5(a)–5(e) show the domain images observed by LMOKE microscopy along the HA for $[Co_{80}Fe_{20}(t = 1.8\ nm)/Al_2O_3(3\ nm)]_9$ for $\mu_0 H = -16$, 1, 3.07, 4.28, and 16 mT, respectively. For better visualization, the corresponding field points have been marked as points 1–5 in the hysteresis loop measured along HA in Fig. 2(b). At negative saturation ($\mu_0 H = -16$ mT), the sample is in its single-domain state, as observed from the uniform gray color of the domain image [Fig. 5(a)]. When the field is reversed ($\mu_0 H = 1$ mT), nucleation of fine domains occurs, which is observed in Fig. 5(b). On further increasing the magnetic field, e.g., at $\mu_0 H = 3.07$ mT, thick, black looplike features (360° DWs) are observed, as shown in the domain image in Fig. 5(c). The zoomed-in image of these features for the highlighted area in Fig. 5(c) is shown in Fig. 5(f). It shows the 360° DWs having the same gray scale on either side of the wall, which implies that the magnetization direction is identical on both sides of these walls. This indicates that the spins inside these walls rotate by 360°. These walls exist even at fields where

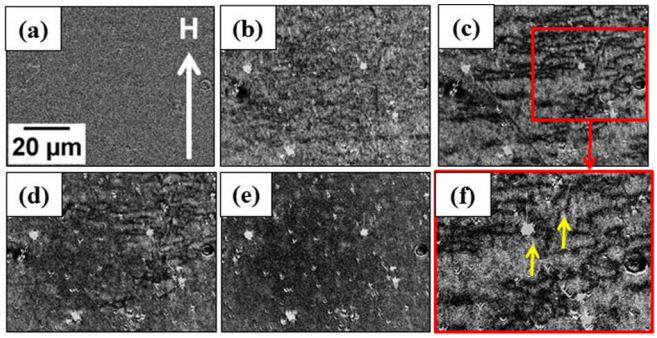

FIG. 5. LMOKE microscopy domain images along the HA for (a) $\mu_0 H = -16$, (b) 1, (c) 3.07, (d) 4.28, and (e) 16 mT. For better visualization, the corresponding field points have been marked in the HA hysteresis loop shown in Fig. 2(b). (f) Zoomed-in ($50 \times 35\ \mu m^2$) domain image of the highlighted area in (c). The thick black looplike features are 360° DWs.

the hysteresis loop closes. For example, at $\mu_0 H = 4$ mT we observe 360° DWs as shown in Fig. 5(d). The nucleation of these 360° DWs during the magnetization reversal for the two branches of the hysteresis is shown in Videos VS2 and VS3 in the Supplemental Material [31]. By applying a high field the 360° DWs are annihilated. The high-field stability is again observed in Fig. 5(e), for which the applied field was $\mu_0 H = 16$ mT, close to the saturation field [see Fig. 2(b)].

The 360° DWs formed along HA in MIMs can be explained by the difference in the sense of the rotation of the magnetization of the grains [17], which occurs due to the orientational dispersion of the anisotropy of grains. In MIMs, the granular thin film is formed by the coalescence of CoFe nanoparticles [6,25]. It was shown in previous reports that for $t < 1.6$ nm CoFe layers are discontinuous, while for $t \geqslant 1.6$ nm the percolation threshold is reached, giving rise to continuous thin films [33]. Therefore, the MIM sample studied here with $t = 1.8$ nm will be dominated by the underlying granular morphology of the film. Hence, in this case the exchange coupling responsible for coherent rotation will not be sufficient to overcome the energy barrier due to the random anisotropy [9].

In order to understand the experimental observation, micromagnetic simulations were performed using the OOMMF software [30] for $[Co_{80}Fe_{20}(t = 1.8\ \text{nm})/Al_2O_3(3\ \text{nm})]_n$, where n corresponds to the number of bilayers. In order to save computational time we have performed detailed micromagnetic simulations for two magnetic layers, i.e., $n = 2$. Nevertheless, we have also performed several simulations for $n = 9$ and found that the results are consistent. Therefore, our interpretation from the series of simulations made for the case of two magnetic layers can be extended to the sample studied experimentally in this work.

The lateral size of the sample was 304×304 nm^2. The cell size was defined to be $3.2 \times 3.2 \times 1.8$ nm^3. The value of exchange energy used in the OOMMF simulations was 10.3×10^{-12} J/m. The saturation magnetization was assumed to be 1.44×10^6 A/m, which corresponds to bulk cobalt. The model is based on minimization of the energy, Eq. (3), by respecting the Landau-Lifshitz-Gilbert equation of motion of the magnetization [34].

As mentioned above, the sample studied in this work exhibits uniaxial anisotropy K_u and a non-negligible random anisotropy K_r. Therefore, in addition to the uniaxial anisotropy K_u we introduced a random anisotropy term K_r in the OOMMF simulation. That is, each individual simulation cell, which represents exactly one grain, exhibits two anisotropy terms. The uniaxial term is constant in magnitude and direction for all cells. However, the random anisotropy term has a constant magnitude for each cell but a direction which is drawn randomly from a unit sphere using mathematical algorithms implemented in the OOMMF code. The latter accounts for the directional dispersion in local anisotropy of the grains in the real sample. Figure 6 shows the simulated hysteresis and the domain images for comparison of different values of K_u and K_r along the EA. Three cases are shown in Fig. 6 in which K_u is equal to K_r (case I), K_u and K_r are comparable (case II), and K_u is stronger than K_r (case III). The domain images for the field points marked in the hysteresis from A to F for cases I, II, and III are shown and marked as A_1, A_2 to F_1, F_2, respectively. The suffixes 1 and 2 for each domain image refer to the bottom and top cobalt layers, respectively. The red and blue pixels in the images denote magnetization $M_x < 0$ and $M_x > 0$, respectively. The simulations were performed by negatively saturating the sample and then reversing the field towards positive direction.

It was found that 360° DWs were formed when either $K_u = K_r = 0.1 \times 10^6$ J/m^3 (Fig. 6, case I) or $K_u = 0.15 \times 10^6$ J/m^3 and $K_r = 0.1 \times 10^6$ J/m^3 (Fig. 6, case II), i.e., when uniaxial and random anisotropies are comparable ($K_u \sim K_r$). It can be observed from Fig. 6 that 360° DWs were formed in the Co_2 (i.e., top cobalt) layer for cases I and II, depicted by domain images C_2 and D_2, respectively. The blue color on either side of these DWs denotes the same magnetization direction on both sides of the walls. This simulation result is in accordance with the XPEEM and Kerr microscopy observations.

The spins inside these walls rotate by 360°, as shown in Fig. S1 in the Supplemental Material [31], which is a zoomed-in view of the wall obtained from OOMMF simulations. The formation of 360° DWs results from a combination of two 180° Néel walls. These 360° DWs require larger fields (compared to the switching field) for annihilation, as can be observed at field point E in the insets in Fig. 6 (for cases I and II). Again, this evidences the anomalous stability of double DWs due to repulsive magnetostatic fields, as discovered previously [32]. Very likely, the extraordinary stability of these 360° DWs (fragments) is due to magnetostatic fields giving rise to dipolar repulsion of the 360° DW core from the antiparallel magnetized environment. Simultaneously, deroughening of the 360° DWs is observed (Figs. 3, 4, and S3), similar to what is observed in the creep regime of a thin Co layer with perpendicular anisotropy [32]. It evidences strong correlations between two one-dimensional walls moving in a random potential but bound through forces derived from the dipolar interaction energy. The dipolar repulsion increases the effective line tension for small wall separations, resulting in a stable, long-lived state, in which both walls are flat over long distances. For better visualization of the formation and annihilation of 360° DWs during magnetization reversal for cases I and II see Videos VS4 and VS5 in the Supplemental

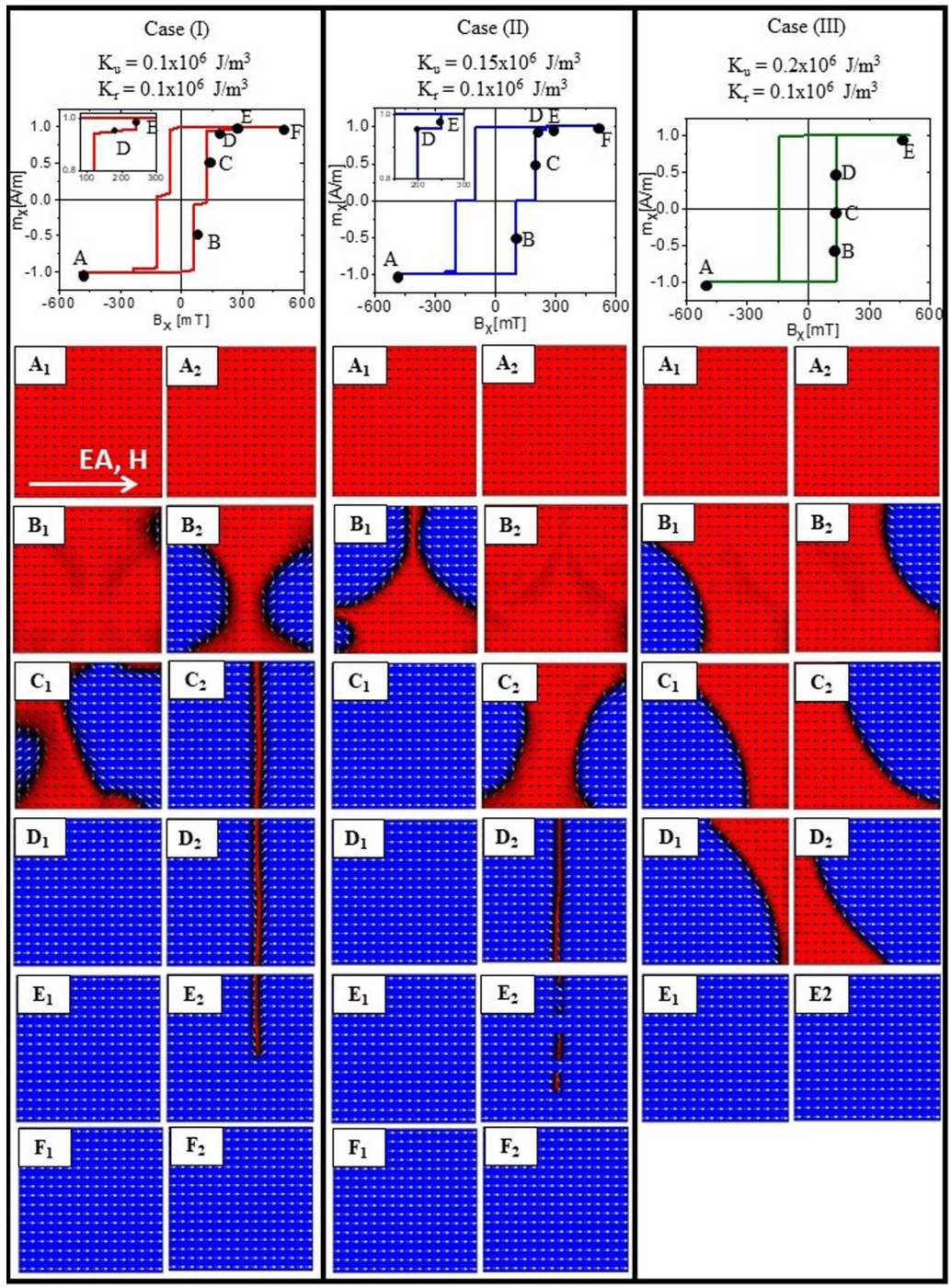

FIG. 6. Simulated hysteresis and corresponding domain images for $[Co(1.8\ nm)/Al_2O_3(3.6\ nm)]_2$ along EA by considering different values of uniaxial (K_u) and random (K_r) anisotropies for formation of 360° DWs. The values of K_u and K_r are as follows: in case I, $K_u = K_r = 0.1 \times 10^6$ J/m^3; in case II, $K_u = 0.15 \times 10^6$ J/m^3 and $K_r = 0.1 \times 10^6$ J/m^3 ($K_u \sim K_r$); and in case III, $K_u = 0.2 \times 10^6$ J/m^3 and $K_r = 0.1 \times 10^6$ J/m^3 ($K_u \gg K_r$). The suffixes 1 and 2 for each domain image refer to the bottom and top cobalt layers, respectively. The red and blue colors in the images denote magnetization $M_x < 0$ and $M_x > 0$, respectively.

Material, respectively [31]. Further, on increasing the field to a very high value (at point F), the sample gets saturated, as is evident from the blue pixels in image F_2 for both cases I and II.

For case III where $K_u \gg K_r$, i.e., $K_u = 0.2 \times 10^6$ J/m^3 and $K_r = 0.1 \times 10^6$ J/m^3 (Fig. 6), no 360° DWs were formed. However, due to the dipolar coupling between the Co layers, mirrored domains were formed, as observed in domain images B_1, B_2 to D_1, D_2 for case III in Fig. 6. For better visualization of this magnetization reversal, see Video VS6 in the Supplemental Material [31]. Hence, the formation of 360° DWs along EA (for cases I and II) can

be attributed to the competing effects of uniaxial and random anisotropies.

Micromagnetic simulations were performed along the HA as well for case II. Along the HA, the reversal is not due to domain wall motion but to coherent rotation. In this case, with the random anisotropy being comparable to the uniaxial one, the exchange interaction cannot outweigh it, and hence, the magnetic moments (or magnetization of domains formed at remanence) rotate oppositely to form the 360° DWs (see Fig. S2 in the Supplemental Material [31]).

In order to understand the effect of interlayer coupling on the formation of 360° DWs similar OOMMF simulations were also performed for two Co (1.8 nm) layers separated by a thicker (108 nm) spacer of Al_2O_3 with $K_u = 0.15 \times 10^6$ J/m^3 and $K_r = 0.1 \times 10^6$ J/m^3. Formation of 360° DWs was also observed for such a case (see Fig. S3 in the Supplemental Material [31]). Since the spacer with this thickness is very large, the effect of interlayer dipolar coupling for the formation of 360° DWs must be negligible in this case.

We further performed simulations on Co (1.8 nm) single layers with the same parameters as mentioned above. The 360° DWs were also observed for this case (see Fig. S4 in the Supplemental Material [31]). Hence, these results indicate that the formation of 360° DWs is governed by the competing effects of uniaxial and random anisotropies. The discussion of the two Co layers given so far also holds for multilayers of $[Co_{80}Fe_{20}(t = 1.8\ \text{nm})/Al_2O_3(3\ \text{nm})]_9$, which approximately mimics the real sample. The corresponding OOMMF simulation was performed along the EA considering the values for case II. The hysteresis and the domain images near the coercive field for $[Co(t = 1.8\ \text{nm})/Al_2O_3(3.6\ \text{nm})]_9$ are shown in Figs. S5(a) and S5(b)–S5(i) in the Supplemental Material, respectively [31]. The formation of 360° DWs similar to those in case II described in Fig. 6 is observed in Figs. S5(d) and S5(e) [31], where a few Co layers exhibit 360° DWs.

IV. CONCLUSIONS

In summary, formation of 360° DWs was observed with XPEEM and LMOKE microscopy in metal-insulator multilayers of $[Co_{80}Fe_{20}(t = 1.8\ \text{nm})/Al_2O_3(3\ \text{nm})]_9$. Micromagnetic simulations suggest that formation of 360° DWs can be attributed to the uniaxial anisotropy and the presence of orientational dispersion of local random anisotropy. Along the EA, the 360° DWs are formed by the merger of two 180° DWs. However, along the HA 360° DWs are formed as the magnetic moments do not rotate coherently with sweeping the magnetic field. When such a random distribution of anisotropy axes being modeled by a random anisotropy term (K_r) in the simulations is comparable to the uniaxial anisotropy, the exchange anisotropy contribution is not outweighed. This results in an opposite sense of rotation of the magnetic moments, leading to the formation of 360° DWs. Therefore, we show that apart from other reasons, 360° DWs can be formed due to the competing effects of uniaxial and random anisotropies present in magnetic thin films. We have shown that the interlayer coupling effect has a negligible effect on the formation of 360° DWs. Further, in this work we have considered a simple approach to mimic the dispersion in anisotropy by K_r, which has a fixed magnitude, and its direction changes from cell to cell. However, a more appropriate approach for K_r would be to consider a fixed magnitude but apply a weighting function for the direction of each grain [35]. Further, the size of the grains in the sample may have a significant effect on the formation of such 360° DWs. Therefore, a systematic simulation may be performed in the future to elucidate these effects on the 360° DW physics.

ACKNOWLEDGMENTS

We thank the Department of Atomic Energy (DAE) and Nanomission Department of Science and Technology (DST)–Nanomission [Project No. SR/NM/NS1088/2011(G)] of the government of India for financial support. This research used resources of the Advanced Light Source, which is a DOE Office of Science User Facility under Contract No. DE-AC02-05CH11231. We thank HZB for the allocation of synchrotron radiation beam time.

[1] M. N. Baibich, J. M. Broto, A. Fert, F. Nguyen Van Dau, F. Petroff, P. Etienne, G. Creuzet, A. Friederich, and J. Chazelas, Phys. Rev. Lett. **61**, 2472 (1988).
[2] G. Binasch, P. Grünberg, F. Saurenbach, and W. Zinn, Phys. Rev. B **39**, 4828(R) (1989).
[3] P. Weiss, J. Phys. Theor. Appl. **6**, 661 (1907).
[4] M. Getzlaff, *Fundamentals of Magnetism* (Springer, Berlin, 2007), Chap. 7.
[5] D. O. Smith, M. S. Cohen, and G. P. Weiss, J. Appl. Phys., **31**, 10 (1960).
[6] W. Kleemann, O. Petracic, Ch. Binek, G. N. Kakazei, Yu. G. Pogorelov, J. B. Sousa, S. Cardoso, and P. P. Freitas, Phys. Rev. B **63**, 134423 (2001).
[7] S. Bedanta, T. Eimüller, W. Kleemann, J. Rhensius, F. Stromberg, E. Amaladass, S. Cardoso, and P. P. Freitas, Phys. Rev. Lett. **98**, 176601 (2007).
[8] M. Takahashi and T. Kono, J. Phys. Soc. Jpn. **15**, 936 (1960).
[9] O. Idigoras, A. K. Suszka, P. Vavassori, P. Landeros, J. M. Porro, and A. Berger, Phys. Rev. B **84**, 132403 (2011).
[10] M. S. Cohen, J. Appl. Phys. **34**, 1221 (1963).
[11] R. Alben, J. J. Becker, and M. C. Chi, J. Appl. Phys. **49**, 1653 (1978).
[12] G. Herzer, IEEE Trans. Magn. **26**, 1397 (1990).
[13] A. Hubert and R. Schäfer, *Magnetic Domains: The Analysis of Magnetic Microstructures* (Springer, Berlin, 2008).
[14] H. S. Cho, C. Hou, M. Sun, and H. Fujiwara, J. Appl. Phys. **85**, 8 (1999).
[15] L. J. Heyderman, H. Niedoba, H. O. Gupta, and I. B. Puchalska, J. Magn. Magn. Mater. **96**, 125 (1991).
[16] L. J. Heyderman, J. N. Chapman, and S. S. P. Parkin, J. Appl. Phys. **76**, 6613 (1994).
[17] K. J. O'Shea, K. Rode, H. Kurt, D. McGrouther, and D. A. MacLaren, J. Phys D **48**, 055001 (2015).

[18] R. H. Wade, Philos. Mag. **103**, 49 (1964).
[19] C. B. Muratov and V. V. Osipov, J. Appl. Phys. **104**, 053908 (2008).
[20] M. Hehn, D. Lacour, F. Montaigne, J. Briones, R. Belkhou, S. El Moussaoui, F. Maccherozzi, and N. Rougemaille, Appl. Phys. Lett. **92**, 072501 (2008).
[21] A. L. Gonzalez Oyarce, T. Trypiniotis, P. E. Roy, and C. H. W. Barnes, Phys. Rev. B **87**, 174408 (2013).
[22] Y. Jang, S. R. Bowden, M. Mascaro, J. Unguris, and C. A. Ross, Appl. Phys. Lett. **100**, 062407 (2012).
[23] M. J. Liedke, K. Potzger, A. H. Bothmer, J. Fassbender, B. Hillebrands, M. Rickart, and P. P. Freitas, J. Appl. Phys. **100**, 043918 (2006).
[24] M. Diegel, R. Mattheis, and E. Halder, IEEE Trans. Magn. **40**, 4 (2004).
[25] G. N. Kakazei, Yu. G. Pogorelov, A. M. L. Lopes, J. B. Sousa, S. Cardoso, P. P. Freitas, M. M. Pereira de Azevedo, and E. Snoeck, J. Appl. Phys. **90**, 4044 (2001).
[26] X. Chen, S. Bedanta, O. Petracic, W. Kleemann, S. Sahoo, S. Cardoso, and P. P. Freitas, Phys. Rev. B **72**, 214436 (2005).
[27] S. Bedanta, O. Petracic, E. Kentzinger, W. Kleemann, U. Rücker, A. Paul, Th. Brückel, S. Cardoso, and P. P. Freitas, Phys. Rev. B **72**, 024419 (2005).
[28] J. Stöhr, H. A. Padmore, S. Anders, T. Stammler, and M. R. Scheinfein, Surf. Rev. Lett. **5**, 1297 (1998).
[29] F. Kronast, J. Schlichting, F. Radu, S. K. Mishra, T. Noll, and H. A. Dürr, Surf. Interface Anal. **42**, 1532 (2010).
[30] M. J. Donahue and D. G. Porter, *OOMMF User's Guide* (National Institute of Standards and Technology, Gaithersburg, MD, 1999).
[31] See Supplemental Material at http://link.aps.org/supplemental/10.1103/PhysRevB.98.134440 for better visualization of 360° DWs in XPEEM, MOKE microscopy, and OOMMF. A zoom-in image of magnetic moments inside the 360° DWs and additional OOMMF simulations are also given.
[32] M. Bauer, A. Mougin, J. P. Jamet, V. Repain, J. Ferré, R. L. Stamps, H. Bernas, and C. Chappert, Phys. Rev. Lett. **94**, 207211 (2005).
[33] S. Bedanta, E. Kentzinger, O. Petracic, W. Kleemann, U. Rücker, Th. Brückel, A. Paul, S. Cardoso, and P. P. Freitas, Phys. Rev. B **74**, 054426 (2006).
[34] A. Aharoni, *Introduction to the Theory of Ferromagnetism* (Clarendon, Oxford, 1996).
[35] W. Scholz, D. Suess, T. Schrefl, and J. Fidler, J. Appl. Phys. **95**, 6807 (2004).